Sensitivity Analysis of Convection of the 24 May 2002 IHOP Case Using Very Large Ensembles

WILLIAM J. MARTIN

Center for Analysis and Prediction of Storms, Norman, Oklahoma

MING XUE

Center for Analysis and Prediction of Storms, and School of Meteorology, University of Oklahoma, Norman, Oklahoma

(Manuscript received 20 September 2004, in final form 13 May 2005)

ABSTRACT

This paper introduces the use of very large ensembles for detailed sensitivity analysis and applies this technique to study the sensitivity of model forecast rainfall to initial boundary layer and soil moisture fields for a particular case from the International H_2O Project (IHOP_2002) field program. In total, an aggregate ensemble of over 12 000 mesoscale model forecasts are made, with each forecast having different perturbations of boundary layer moisture, boundary layer wind, or soil moisture. Sensitivity fields are constructed from this ensemble, producing detailed sensitivity fields of defined forecast functions to initial perturbations. This work is based on mesoscale model forecasts of convection of the 24 May 2002 IHOP case, which saw convective initiation along a dryline in western Texas as well as precipitation along a cold front. The large ensemble technique proves to be highly sensitive, and both significant and subtle connections between model state variables are revealed. A number of interesting sensitivity results are obtained. It is found that soil moisture and ABL moisture have opposite effects on the amount of precipitation along the dryline; that moisture on both the dry and moist sides of the dryline was equally important; and that some small perturbations were alone responsible for entire convective storm cells near the cold front, a result implying a high level of nonlinearity. These sensitivity analyses strongly indicate the importance of accurate low-level water vapor characterization for quantitative precipitation forecasting.

1. Introduction

One goal of the International H_2O Project (IHOP_2002; 13 May through 25 June 2002; Weckwerth et al. 2004) is to improve the prediction of convection and the associated precipitation through improved low-level water vapor characterization. This paper attempts to address this issue by analyzing the sensitivity of a model forecast for an IHOP case (the 24 May 2002 convective initiation case) to small perturbations in the atmospheric boundary layer (ABL) fields and surface moisture at the initial model time. This is accomplished by testing a large set of possible initial ABL perturbations to fields of water vapor mixing ratio (q_v), volumetric soil moisture content (q_s), and meridional wind component (v). The number of initial perturbations tested is large (over 2000 for each variable), requiring a large number of forward model runs, which could only be accomplished in a reasonable amount of time by using a large parallel computing system. From these sets of perturbed runs, detailed sensitivity fields are constructed. The model used is the Advanced Regional Prediction System (ARPS; Xue et al. 2000, 2001, 2003), a multiscale nonhydrostatic atmospheric modeling system.

The sensitivity fields constructed in the paper are analogous to those produced by adjoint models (Kim et al. 2004; Kleist and Morgan 2005; Errico and Vukicevic 1992; Errico 1997; Hall and Cacuci 1982, 1983). However, adjoint methods are difficult to implement for complex models, especially those employing complex physical parameterizations (Errico 2003). Also, because adjoints are linear models, adjoint-derived sensitivities can fail to be meaningful if long time integrations are involved where nonlinearities in the model become im-

Corresponding author address: Dr. William Martin, Center for Analysis and Prediction of Storms, 100 East Boyd, SEC Room 1110, Norman, OK 73019.
E-mail: wjmartin@ou.edu

portant. For these reasons, explorations of forecast sensitivities have sometimes taken the approach of using a number of direct model integrations (e.g., Crook 1996; Mullen and Baumhefner 1994). Because of limitations in computational power, these sensitivity analyses from forward model runs have necessarily been limited to a small number (10 to 100) of model runs. Sensitivity fields are useful for understanding predictability, for understanding physical connections between variables, and for use in data assimilation where model initial fields are adjusted using forecast sensitivities.

The availability of large parallel computer systems with thousands of processors now makes it possible to obtain sensitivity fields from a very large number (thousands) of nonlinear forward model runs with full physics, with each model run having a small perturbation at a different location in space. Small, spaced perturbations at a large number of locations can be used, and sensitivity fields can be constructed from such very large ensembles (VLE) of model runs. The number of perturbations necessary to characterize the entire three-dimensional model space is proportional to the number of degrees of freedom in the model, that is, the number of input variables times the number of grid points. This would still be too many perturbed model runs to make for even for the most powerful of modern supercomputers. Consequently, this method is only viable for calculating two-dimensional sensitivity fields. An exploration of the sensitivity of a forecast to (two-dimensional) ABL fields and surface soil model fields is an appropriate application of the VLE technique.

It is instructive to note the similarities and differences between the VLE technique and the adjoint technique. They both calculate the same dimensional sensitivity of a defined response function of a forecast, J (which might be, e.g., the total rainfall in some area), to an initial model state variable, a_0 (where a_0 might be the initial field of ABL moisture), $(\partial J/\partial a_0)$. To calculate $(\partial J/\partial a_0)$, the VLE technique uses a small perturbation in a_0 and calculates the change in J by calculating the difference between the perturbed and unperturbed runs. The adjoint method uses the actual mathematical derivative of the model and directly calculates $(\partial J/\partial a_0)$ (essentially through many recursive applications of the chain rule for differentiation). The adjoint, therefore, gives the exact sensitivity for infinitesimal perturbations, while the VLE technique gives the actual sensitivity for a finite perturbation. If the perturbation size used in the VLE technique is sufficiently small, then the two techniques, in principle, give the same result, and comparing the two techniques is a common method of checking the adjoint implementation. Nonlinearity of the model, however, can lead to different results even for relatively small perturbations. There is also a minimum to the size of the perturbations that can be used in the VLE technique because of round-off error.

Another limitation of the VLE technique relative to the adjoint method is that the perturbations chosen for the VLE cannot be truly exhaustive due to limitations in computational resources. For this study, we perturb boundary layer moisture, but we do not perturb upper-level winds, for example. This means that, while we can determine the sensitivity of any forecast response function to boundary layer moisture, we cannot determine the sensitivity of such functions to upper-level winds, or to anything we did not perturb. If one is searching for the largest source of sensitivity, then it might be missed if it lay in some variable or region not perturbed. Adjoints, in contrast, automatically produce complete sensitivity fields that can be searched for the largest sources of sensitivity, as was done, for example, by Fovell (2004).

Section 2 introduces briefly the case, the ARPS model, and its configuration used for the forecast, and provides the details of the VLE technique. The results are presented in section 3, and a summary is given in section 4, together with additional discussion.

2. The ARPS model and the VLE technique

a. The 24 May 2002 case, the ARPS configuration, and the initial condition

A forecast was made from initial fields at 1800 UTC on 24 May 2002. This is local noon for the study area in the southern Great Plains of the United States. The initial fields were obtained by interpolation from the 40-km resolution Eta analysis at 1800 UTC. The interpolation was done to a $135 \times 135 \times 53$ (x, y, z, respectively) grid with a 9-km horizontal grid spacing, centered over the IHOP study area in the southern Great Plains. The model used a vertically stretched grid with a minimum spacing at the surface of 20 m, and a maximum height of about 20 km. The first level above the ground was, therefore, at 10 m above the ground. The time step size was 15 s. Figure 1 shows the initial surface (10-m elevation) fields of water vapor and wind.

We employed the ARPS model using leapfrog time differencing, fourth-order centered advection in both the horizontal and vertical directions, and a mode-split with vertically implicit treatment for acoustic waves. Fourth-order computational mixing is included to suppress small-scale noise, and a 6-km-thick Rayleigh damping layer is applied near the upper boundary. The lateral boundaries are forced by boundary conditions obtained from temporal and spatial interpolations of

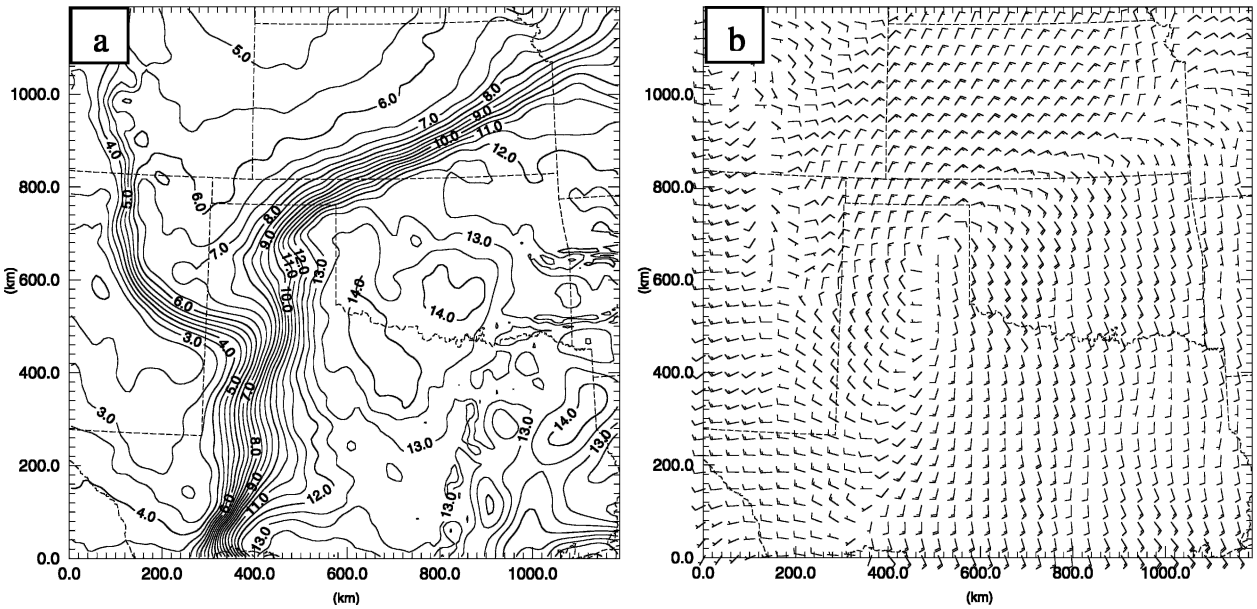

FIG. 1. Initial fields used for the ARPS model from 24 May 2002 at 1800 UTC. (a) Initial surface 10-m water vapor field in g kg^{-1}. (b) Initial field of 10-m wind barbs. One full wind barb is 5 m s^{-1} and a half wind barb is 2.5 m s^{-1}. One-fourth of the available wind barbs are shown.

the 1800 UTC 40-km horizontal-resolution Eta forecast at 3-h intervals.

The ARPS model contains many physical parameterization schemes, which can give a high degree of physical realism to forecasts. For this work, we used the following physical parameterizations: full ice microphysics including cloud, rain, ice, snow, and hail variables; a complex long- and shortwave radiation transfer parameterization; stability-dependent surface fluxes; a two-layer force–restore-type soil–vegetation model including soil moisture and soil temperature as prognostic variables, a nonlocal turbulent kinetic energy (TKE)-based PBL parameterization scheme, a 1.5-order TKE-based subgrid-scale turbulence model; and detailed terrain and land surface characteristics definitions. The two-layer soil model includes a surface layer and a 1-m-deep soil layer. The soil and vegetation types and other land surface characteristics were derived from a 1-km database; in addition, three soil types were defined for each grid cell, each carrying a percentage weighting derived from the data. More details on the model and physical parameterizations can be found in the ARPS description papers (Xue et al. 2000, 2001, 2003).

Convective and cumulus parameterization schemes are available in ARPS, but were not used for this study even though, with a 9-km horizontal resolution, the model is not expected to be able to represent convective cells with complete realism. Convective parameterization has limitations as well, and preliminary forecast runs of this case with explicit convection appeared more realistic and agreed better with the observed fields than runs using convective parameterization. Consequently, the decision was made not to include convective parameterization. The results of the unperturbed control run are qualitatively similar to the 3- and 1-km-resolution simulations of the same case done by Xue and Martin (2006). Running all of the forward runs at 3-km resolution would have been too expensive computationally.

All forward model runs were made for 6 h from the 1800 UTC 24 May initial condition to 0000 UTC 25 May. The unperturbed model forecast fields of 10-m water vapor and wind vectors are shown in Fig. 2. Figure 3a shows the vertically integrated liquid water field at the forecast time, and Fig. 3b shows the total accumulated rainfall through 6 h.

While an attempt at a high degree of agreement with the observed convection was not made, this forecast is similar in many respects to the actual weather on 24 May 2002. The observations are described in great detail elsewhere (e.g., Wakimoto et al. 2006; Holt et al. 2006; Xue and Martin 2006) and will not be repeated in detail here. Figure 1 shows the general situation at 1800 UTC before any convection has occurred. A dryline was oriented north–south from the central-eastern Texas panhandle southward, and a cold front existed from the central-eastern Texas panhandle northeastward through eastern Kansas. A triple-point low ex-

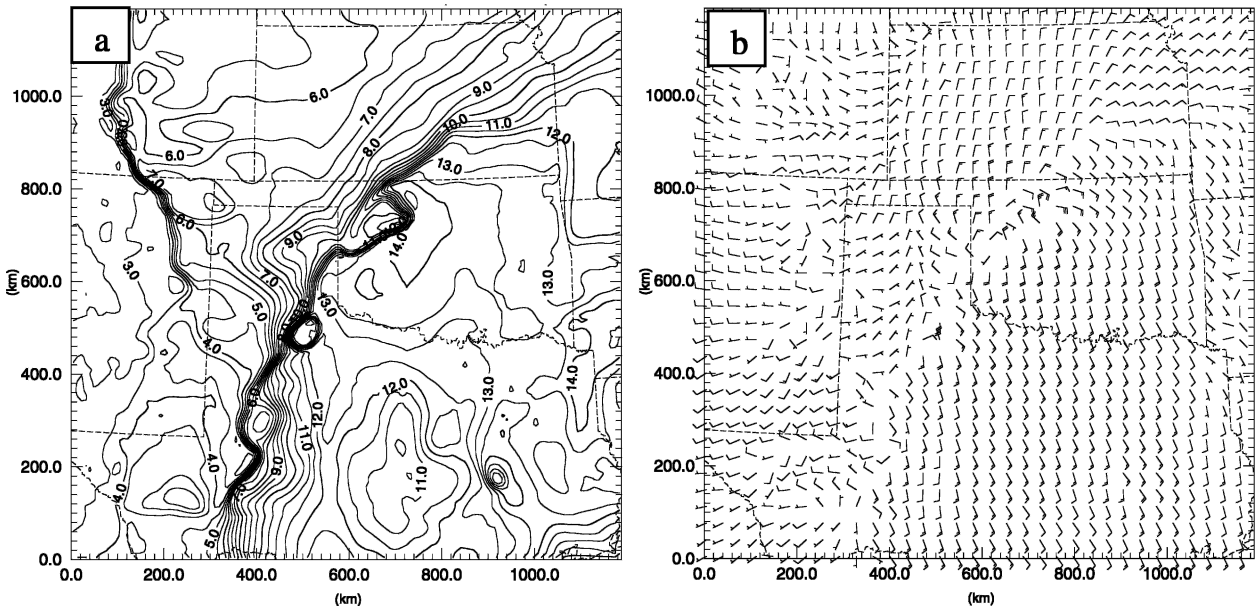

FIG. 2. Six-hour forecast fields from integration of the ARPS model, valid at 0000 UTC, 25 May 2002. (a) Surface 10-m water vapor field in g kg^{-1}, and (b) field of 10-m wind barbs. One full wind barb is 5 m s^{-1} and a half wind barb is 2.5 m s^{-1}. One-fourth of the available wind barbs are shown.

isted at the intersection of the dryline and cold front. After 6 h for the real atmosphere, the triple point had moved southeastward and convection initiated at about 2030 UTC in northwest Texas south of the triple point. The ARPS forecast presented here in Figs. 2 and 3 captured the location of convective initiation along the dryline accurately, although it initiated convection later than observed, and by 0000 UTC 25 May, much less convection occurred in the model than in the actual atmosphere. Also, the model has more rain near the

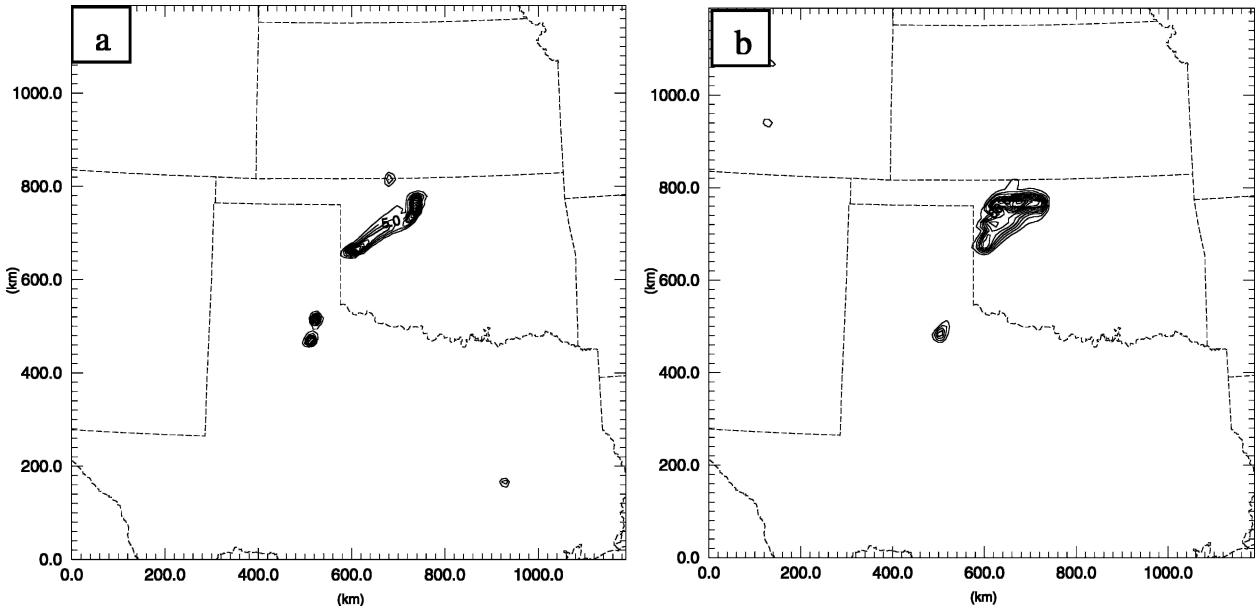

FIG. 3. Forecast precipitation fields after 6 h of integration. (a) Vertically integrated liquid water (cloud plus rain). Contour increments are 2.5 kg m^{-2} with a maximum of 35. (b) Total accumulated precipitation. Contour increments are 15 mm with a maximum of 200 mm.

cold front in northwestern Oklahoma than was observed. Despite particular differences between the model forecast and the observations, useful sensitivity analyses of details of convection along the cold front and dryline in the model forecast can be made.

b. The very large ensemble technique

To calculate the sensitivity field of the model forecast to the initial fields, we use an exhaustive range of perturbed forward model runs. In each run, a perturbation of one initial field variable in a different location is made. The sensitivity field is then assembled from this ensemble of forward model runs.

If the initial variable in question is the temperature at one specific location, T_{1i}, and the forecast of interest is the temperature at a later time at another specific location, T_{2f}, then the sensitivity could be found by perturbing T_{1i} by a small amount δT_{1i}, determining the change in the forecast, δT_{2f}, and dividing, yielding $\delta T_{2f}/\delta T_{1i}$. If we wanted to find the sensitivity (or impact) of a perturbation in T_{1i} on the entire forecast temperature field, then we need to merely perturb T_{1i} as before, run the model to the forecast time, and determine the change in forecast temperature at each grid location of the model. The change in the forecast field can be plotted, for example, as a contour map, thus visualizing the impact of a perturbation in T_{1i}. The sensitivity field of a specific forecast scalar is much more difficult to construct. For example, if we wanted to find the sensitivity of the forecast temperature at a specific location, T_{2f} to the entire initial field of temperature by using perturbed model runs, then we need to run one forward perturbed model run for each grid location of the model. If the model has N grid points with independent initial temperature values, then we need N forward model runs so that the dependence of T_{2f} on the value of initial temperature at each location can be found.

Considering just a $135 \times 135 \times 53$ grid with potentially six primitive variables that one might be interested in perturbing (three wind components, pressure, temperature, and water vapor), there are nearly six million possible ways a single perturbation could be added to the initial condition to test its impact. It is also possible to vary the magnitude of the perturbation, leading to a further multiplication of potential perturbations to examine. It is not practical to try this many perturbations with current computers. To reduce this number to one practically manageable, we selected to perturb only certain variables in a two-dimensional surface layer. We chose to make the perturbations 27 km by 27 km in horizontal size (three grid cells by three grid cells) and 1 km in vertical depth at the surface (or 1 m in depth for soil moisture). The horizontal domain can be completely covered by placing nonoverlapping perturbations of this size onto 2025 different horizontal places on the grid at the initial time (the 2025 total is found by dividing the 135 by 135 grid into a 45 by 45 grid). The 1-km depth for the perturbation is chosen because it approximates the depth of the ABL for this case at the initial time. We only perturbed water vapor mixing ratio, q_v (which affects the convective available energy and precipitable water), volumetric soil moisture, q_s (which affects latent and sensible heat fluxes into the atmosphere), and meridional wind, v (which affects northward transport of moisture and wind shear) as it is believed that these are the variables that have the greatest impact on precipitation. For the q_s perturbations, both the surface and deep layers were given the same perturbation. To investigate the possibility of nonlinear sensitivity effects, each variable is perturbed with both positive and negative perturbations. In principle, if the sensitivity fields depend linearly on the size of the initial perturbations, then identical results should be obtained by using positive and negative perturbations (after dividing by the perturbation size).

The size of the perturbation must be large enough so that round-off errors in model calculations do not overwhelm the effects of the perturbations. They must also be small enough so that the perturbed model forecast is reasonable. For example, if too large an ABL moisture perturbation were used, condensation in the model would immediately be triggered at the perturbation site, leading to a model forecast quite different from the unperturbed forecast and one which would never have happened with any reasonable-size error in the initial condition. From preliminary tests, it was found that perturbations of about 10% of the magnitude of the unperturbed variable seemed to meet these two criteria. The use of perturbations smaller than a few percent led to excessively noisy sensitivity fields. The magnitude of perturbations was, therefore, chosen to be ± 1 g kg^{-1}, ± 0.01 m^3 m^{-3}, and ± 1 m s^{-1} for q_v, q_s, and v, respectively. Figure 4 shows a sample perturbation in q_v in both horizontal and vertical cross sections. Because of diffusion, these small perturbations are rapidly spread to the surrounding areas, diluting their magnitude. It is only because computer precision is much higher (relative to observations) that their effects could be detected. In this study, single precision was used, which represents values to approximately seven digits. Had double precision been used, it might have been possible to get low-noise sensitivity fields from smaller perturbations, though at the extra cost of using double precision. The use of small perturbations might be useful when comparing with adjoint-derived sensitivities. However, the perturbations used here are typical of

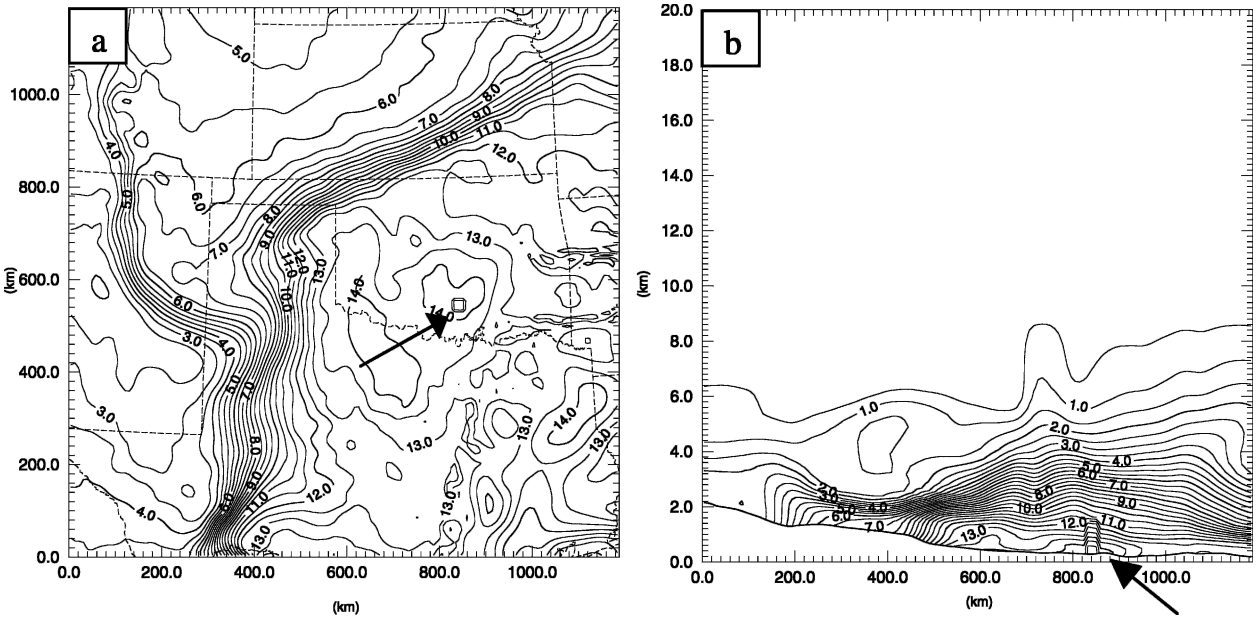

FIG. 4. Sample initial condition the water vapor field perturbed at one location. (a) Surface 10-m water vapor mixing ratio plot with perturbation in south-central Oklahoma. (b) Vertical cross section of water vapor mixing ratio on a zonal plane through the perturbation. Contour increment is 0.5 g kg^{-1}. Arrows point to the location of the initial perturbation.

analysis errors, and allow the model to reveal nonlinearities. For perturbations of this size, single precision was adequate.

Some model perturbations will create initial imbalances in the model. A wind perturbation as done here, for example, would be expected to produce sound waves, which are not in unperturbed runs. However, this effect is genuine and is one of the ways in which the effect of a perturbation in wind at one location spreads throughout the domain. Any sensitivity depending on such adjustments of the model to the perturbations is therefore physically meaningful, though one would expect the sensitivities calculated from effects from acoustic waves to be minor in most cases. The same sensitivities are found from adjoint calculations where the effects of infinitesimal velocity perturbations propagate throughout the domain by way of infinitesimal sound waves.

Table 1 summarizes the six sets of perturbed runs that were made. As each set of perturbed runs took 2025 forward model integrations and there was one unperturbed run, this study involves a total of 12 151 model runs. Each model run takes about 6 h of computer time on one 1-Ghz Alpha processor. Executing thousands of these calculations is, therefore, expensive. Storage of the results from thousands of model runs can also be demanding. Consequently, we only saved the model state at the lowest model level above the surface (10 m) at the final time of the 6-h integration, plus the field of total accumulated precipitation.

These large ensembles of runs were conducted using a large parallel supercomputer at the Pittsburgh Supercomputer Center. This computer consists of over 3000 processors. This problem is highly efficient from a parallelization standpoint as each member of the ensemble is run on one CPU, and the entire ensemble of 2025 members executes in about the same amount of wall-clock time as a single model run (about 6 h). In most cases, each model forecast in each 2025 member ensemble was nearly identical. However, by taking the differences between the unperturbed run and each perturbed run, useful sensitivity fields were constructed.

To assemble a sensitivity field from a set of perturbed runs, a response function, J, is first defined. A response function can be any function of the model forecast. For example, it could be defined as the total precipitation that fell in a certain area. The value of this response function is then calculated from each perturbed model

TABLE 1. Summary of perturbation ensembles.

Perturbation variable	Perturbation value	Typical value of unperturbed variable
q_v, ABL moisture	$+1$ g kg^{-1}	10 g kg^{-1}
q_v, ABL moisture	-1 g kg^{-1}	10 g kg^{-1}
q_s, soil moisture	$+0.01$ m^3 m^{-3}	0.25 kg^3 kg^{-3}
q_s, soil moisture	-0.01 m^3 m^{-3}	0.25 kg^3 kg^{-3}
v, north–south wind	$+1$ m s^{-1}	10 m s^{-1}
v, north–south wind	-1 m s^{-1}	10 m s^{-1}

run and the unperturbed model run, and the value of J from the unperturbed run is then subtracted from that of each perturbed run. This produces a set of changes, δJ, in J. Since each perturbed run had a perturbation at a different location in x–y space, δJ can be thought of as a function of space:

$$\delta J = J_{\text{perturbed}}(x, y) - J_{\text{unperturbed}} = \delta J(x, y), \quad (1)$$

where the spatial location (x, y) is defined by the location of the initial perturbation. Dividing δJ by the size of the initial perturbation, δa_0 (e.g., $\delta a_0 = 1$ g kg^{-1} for q_v perturbations) gives the sensitivity of the scalar J to the field a_0, s, which is an approximation to the exact differential sensitivity:

$$s = \frac{\delta J(x, y)}{\delta a_0} \approx \frac{\partial J}{\partial a_0}(x, y). \quad (2)$$

We note that the response function definition is made after the results from all the perturbed runs have been obtained. This means that a nearly unlimited number of different response functions can be calculated from the same set of perturbed runs. This is a significant advantage over obtaining sensitivity results from an adjoint model, since, with an adjoint, the adjoint model needs to be run separately for each response function definition. In this case, the time it takes to obtain a second J sensitivity field from the VLE is a few seconds, whereas from an adjoint it would take many hours. On the other hand, as mentioned earlier, the VLE technique produces a less complete sensitivity field since, for this study, we are only able to analyze sensitivities to the boundary layer variables perturbed.

It is possible to perturb the model using various patterns of perturbations rather than individual, isolated perturbations. Restricting ourselves only to the 45 by 45 grid of 27 km by 27 km perturbations used here would yield 2^{2025} different possible patterns of perturbations to consider. Since the model is nonlinear, it is possible that a few of these patterns could have strong impacts on the forecast that would never occur with any of the 2025 solitary perturbations. However, since the perturbations are small, such effects are expected to be insignificant, and there is no practical way known to systematically check for such subtle sensitivity patterns.

c. Nondimensionalization and smoothing

Nondimensionalization of the sensitivities is useful for comparing sensitivities of various response functions to various perturbed variables. To do this, the numerator and denominator in (2) are divided by the absolute value of the response function from the unperturbed run, J_0, and the absolute value of the unperturbed input variable, $a_0(x, y)$, respectively. This results in a nondimensional sensitivity, S:

$$S = \frac{\delta J/|J_0|}{\delta a/|a_0|}; \quad (3)$$

thus S is then the fractional change in the response function divided by the fractional change in the perturbed variable. The absolute values are used in nondimensionalization in order to preserve the sign of the sensitivity value. A value of S of 0.1, for example, means that a +1% perturbation in the variable a_0 leads to a +0.1% change in the response function. This nondimensionalization is essentially the same as the relative sensitivity coefficients (RSC) used by Park and Droegemeier (1999). All of the sensitivity plots shown in section 3 have been nondimensionalized. When the perturbation variable is meridional wind, v, more care needs to be taken in nondimensionalization as values of v can be close to zero, making a small perturbation a large fraction of the unperturbed variable, and leading to nondimensional sensitivity values that are unphysically small. For this reason, a minimum value of v of 5 m s^{-1} is used in nondimensionalizing perturbations of v.

In some cases, sensitivity plots have been smoothed by passing the data through a nine-point, diffusive smoother, in some cases multiple times. Smoothing is not used extensively; however, some subtle results are difficult to separate from noise without some smoothing, especially for plots derived from perturbations in q_s and v, which had smaller effects relative to perturbations in ABL moisture, and were therefore impacted more by computer precision.

3. Results

a. Sensitivity effects from advection and diffusion

It is useful to first examine the reasonableness of the results by looking at sensitivities in areas where no active convection occurs. In such areas, advection and diffusion are the primary physical processes operating in the atmosphere and ABL, along with some effects from surface physics and radiation. For Fig. 5a, the response function is defined as the average value of water vapor at 10 m above the surface in the box drawn just south of Oklahoma. Figure 5a plots the nondimensional sensitivity of this response function to initial 1-km-deep +1 g kg^{-1} ABL moisture perturbations. The interpretation of this figure is that a 1% perturbation in q_v in a 1-km-deep by 27 km by 27 km volume at the surface centered at a particular location in the map causes a percentage change in the response function of an amount equal to the contour value at that particular

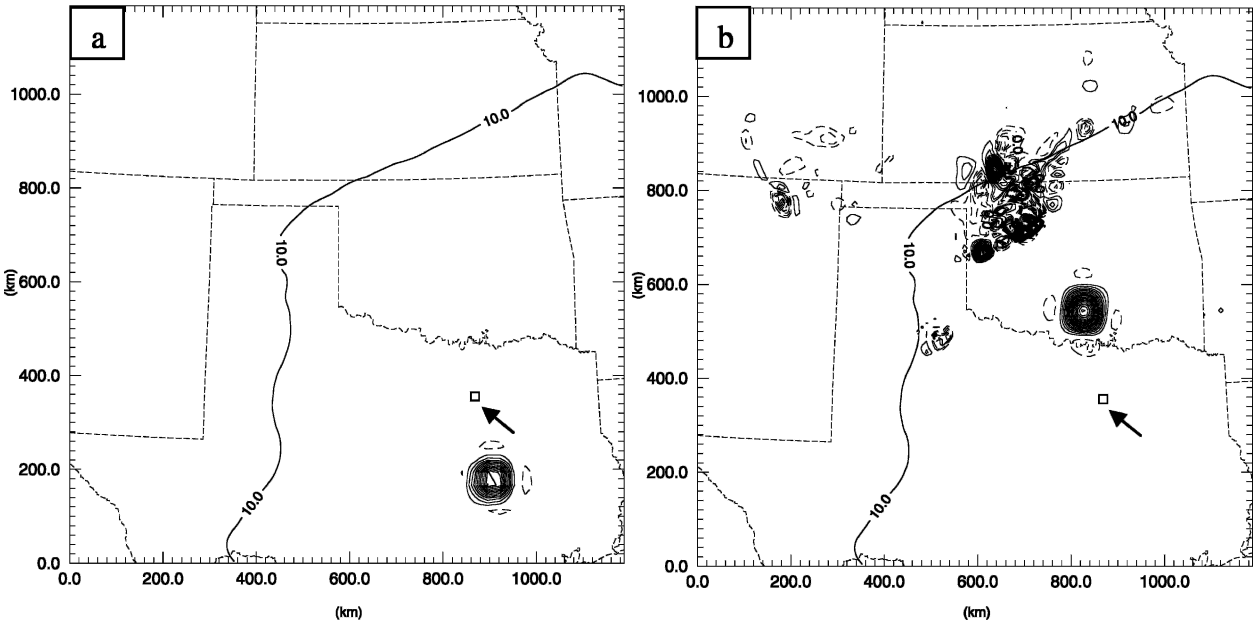

FIG. 5. Nondimensionalized sensitivities of ABL moisture in a region with no precipitation. (a) Sensitivity field showing the dependence of the forecast average 10-m water vapor in the box shown, on initial boundary layer perturbations in water vapor. (b) Sensitivity field showing the change in 10-m water vapor at the 6-h forecast time following an initial boundary layer water vapor perturbation in the box shown. Contour increment is 0.01 and negative contours are dashed. Maximum for (a) is 0.13; local maximum in southern Oklahoma in (b) is 0.18. The 10 g kg^{-1} isopleth of water vapor at 10 m above the ground at the initial model time is drawn for reference in this and all subsequent figures. The location of sensitivity boxes is indicated by the arrow.

location. This figure shows a compact maximum 180 km south of the location where the response function was defined. Given the approximately 10 m s^{-1} of southerly flow in this region (Figs. 1 and 2) and 6 h of model integration, this maximum is approximately what one would expect from diffusion and advection alone. Advection of a moisture perturbation would have moved it by about 200 km, and diffusion spreads the reach of perturbations, so that a broad maximum in sensitivity is found. Also, the maximum in sensitivity of 0.13 agrees well with expectations based on the size of the area of sensitivity. The response function is defined over a 27 km by 27 km area, and we have found a sensitivity area of about 100 km by 100 km. The initial perturbations were also 27 km by 27 km. After the 6 h of integrations, the effects of these perturbations would have spread over a 100 km by 100 km area, diluting their impact by a factor of $27^2/100^2 = 0.07$, which compares with the average of about 0.065 in the maximum area shown in Fig. 5a. In Fig. 5a, we also note secondary minima surrounding the maximum. The contour increment has been deliberately selected small to show these minima. It is thought that these minima are due to a secondary circulation induced by the buoyancy of water vapor perturbations.

For comparison with Fig. 5a, which presents the sensitivity of q_v in a 27-km box to the initial q_v field, Fig. 5b presents the sensitivity of the forecast q_v field to an initial 27-km square and 1-km-deep q_v perturbation. This field is also nondimensional and is calculated by taking the difference between a run with a perturbation at a particular location (indicated by a box drawn in Fig. 5b, which is the same box used for Fig. 5a) and the unperturbed run, dividing by the value of the unperturbed forecast q_v, and then dividing by the fractional size of the perturbation. Figure 5b shows a compact maximum about 200 km downstream of the perturbation location. In addition, Fig. 5b shows forecast changes in q_v at and near areas where convection occurred (as seen in Fig. 3). Evidently, small perturbations in q_v have effects that spread by either acoustic or gravity waves to areas of convection, where this very slight effect is amplified nonlinearly. The actual change in forecast precipitation is slight; it is only the high accuracy of model difference fields that permits this small effect to be resolved. Aside from the amplification of perturbations by convection, Figs. 5a and 5b are notably symmetric, with Fig. 5a showing a compact sensitivity maximum 200 km upstream, and Fig. 5b showing a compact maximum 200 km downstream. This symmetry is due to advection and diffusion being quasilinear to small perturbations and to the fact that the

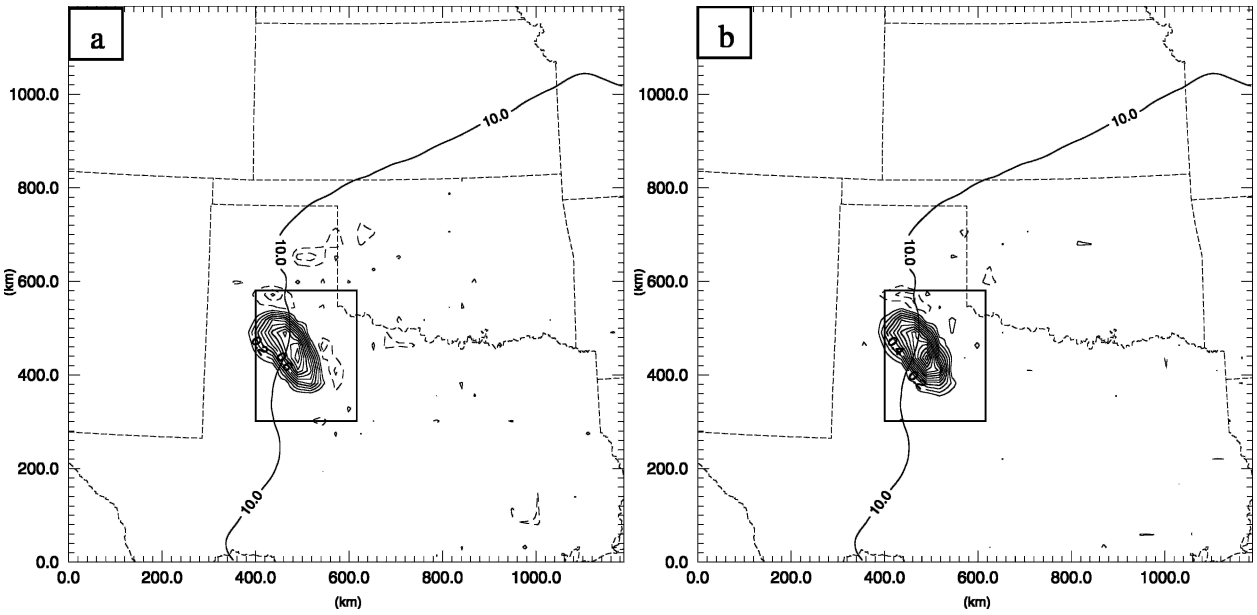

FIG. 6. Sensitivity fields showing the dependence of the total mass of rain that fell in the indicated box on initial 1 g kg^{-1} water vapor boundary layer perturbations. Results from using (a) +1 g kg^{-1} perturbations and (b) −1 g kg^{-1} perturbations. Contour increment is 0.1. Negative contours are dashed. The maximum in (a) is 1.18 and in (b) is 1.47. The 10 g kg^{-1} isopleth of water vapor at 10 m above the ground at the initial model time is drawn for reference.

flow field was quasi-uniform and steady during the period. This observed behavior tends to confirm the correctness of the sensitivity determination procedure.

To test the possibility that the weak minima seen around the principal maxima in Figs. 5a and 5b (which were suggested to be due to a very weak circulation induced by buoyancy) could be due to an artifact from the advection scheme, a test using a monotonic advection scheme (Zalesak 1979) was conducted. The Zalesak scheme is a multidimensional monotonic flux-corrected transport (FCT) scheme that eliminates both undershoots and overshoots associated with conventional advection schemes (in this case a leapfrog centered difference scheme). This test produced a sensitivity plot (not shown) very similar to Fig. 5b, including the weak secondary minima around the principal maxima. This tends to rule out advection errors as the source of this effect.

b. Sensitivity of convection near the dryline

To examine the sensitivity of convection that occurred along the dryline to the perturbed variables, a response function is chosen to be the total mass of precipitation that fell in an area along and ahead (east) of the dryline in the southern Texas panhandle. This area is indicated by the box drawn in Figs. 6–8. As shown by Fig. 3, most of the precipitation that fell in this area was in a small part of the box. The box was made to cover a much larger area than that into which rain fell in the unperturbed run, so as to capture any possible precipitation that may have occurred in some of the perturbed runs at other locations. In practice, the size of the response function box made little difference for sensitivity fields along the dryline so long as it included the region in which rain fell in the unperturbed run, because none of the perturbed runs had significant precipitation at other locations along the dryline.

Figure 6 shows the resulting nondimensional sensitivities calculated from both the +1 g kg^{-1} and −1 g kg^{-1} boundary layer moisture perturbation ensembles. For reference, the 10 g kg^{-1} isopleth of 10-m q_v at the initial model time is also drawn in Fig. 6 and in all other sensitivity plots. This line is close to the initial location of the dryline and cold front. The resulting sensitivity pattern and magnitude from the two sets of ensembles are quite similar with maximum sensitivities of 1.2 and 1.5 for the positive and negative perturbations, respectively. The similarity in the response to positive and negative perturbations implies a degree of linearity in the response to perturbations of this size. In this case, initial moisture perturbations were modifying the amount of precipitation that existed in the unperturbed run, but not creating new areas of precipitation. It is also interesting to note a secondary minimum around the maxima seen in Fig. 6, especially just north of the main area of positive sensitivity, the magnitude of

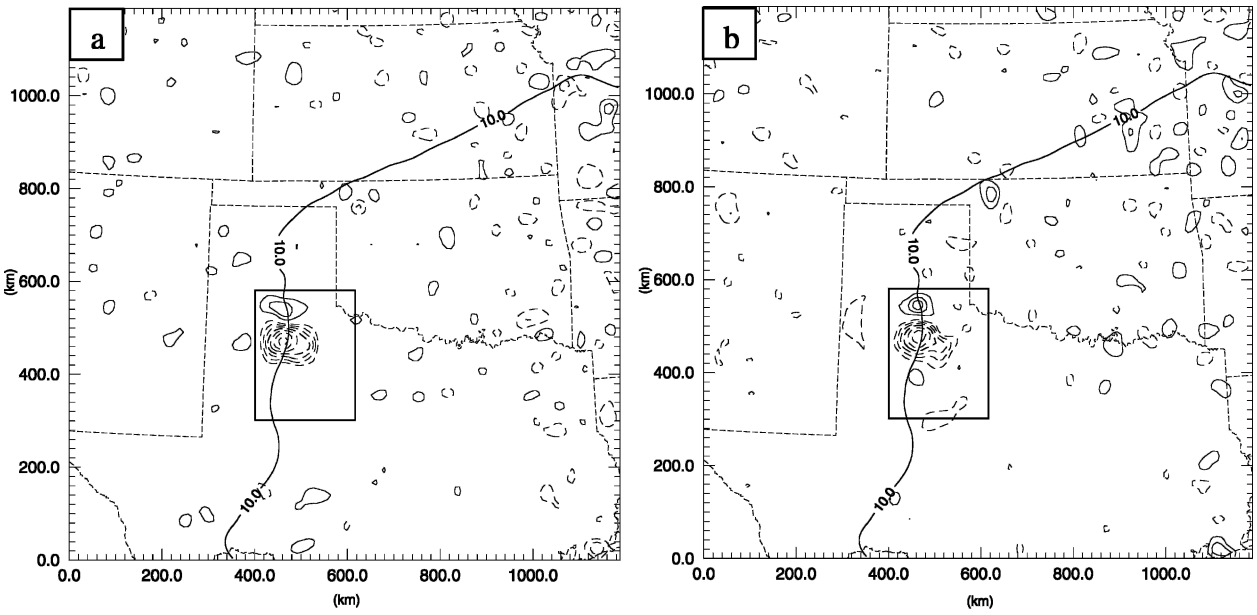

FIG. 7. Nondimensional sensitivity of the total rain that fell in the indicated box to (a) +0.01 $m^3\ m^{-3}$ soil moisture perturbations and (b) −0.01 $m^3\ m^{-3}$ soil moisture perturbations. Contour increment was 0.1. Negative contours are dashed. A nine-point smoother was used once. The minima were −0.74 (−0.85 unsmoothed) and −0.67 (−0.74 unsmoothed) for (a) and (b), respectively. The 10 g kg^{-1} isopleth of water vapor at 10 m above the ground at the initial model time is drawn for reference.

which is about −0.3. The reason for this minimum is not clear, but may be related to a competition effect. A positive moisture perturbation at this minimum may lead to an increase in convection at some location other than within the box, leading to a slight suppression of convection within the box. It is interesting that Fig. 6 shows that the rainfall was equally sensitive to water vapor on both the east and west sides of the 1800 UTC

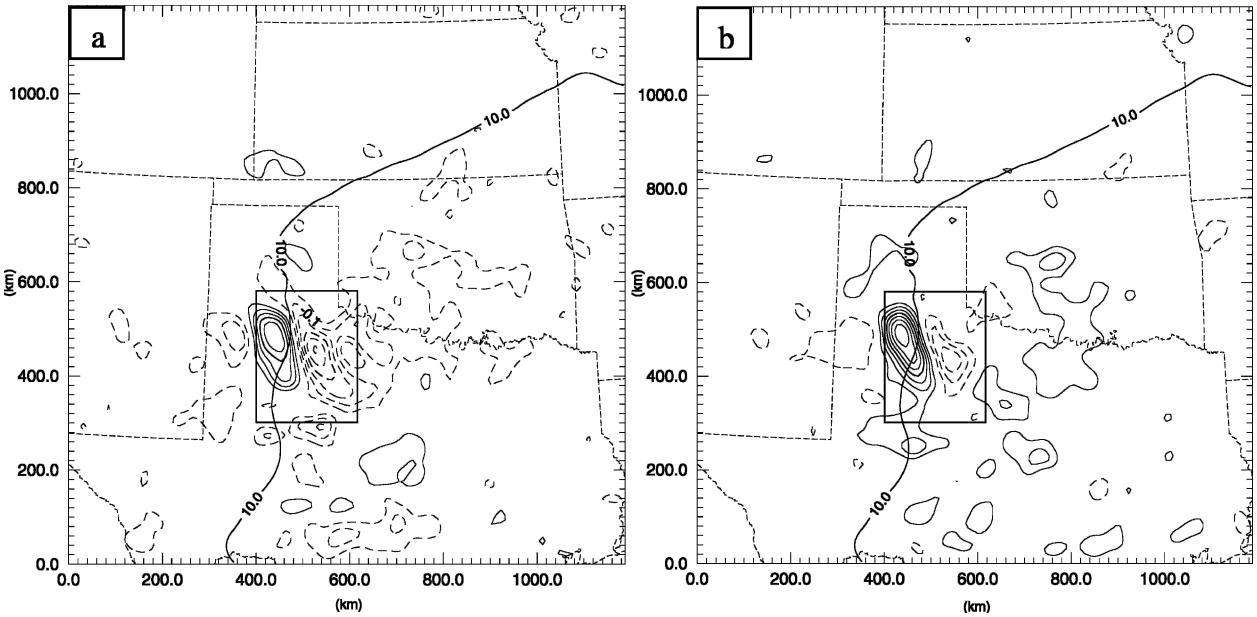

FIG. 8. Nondimensional sensitivity of the total rain that fell in the indicated box to (a) +1 and (b) −1 m s^{-1} ABL v perturbations. Contour increment was 0.025. Negative contours are dashed. A nine-point smoother was used three times. The minima were −0.15 (−0.21 unsmoothed) and −0.10 (−0.15 unsmoothed), and the maxima were 0.15 (0.19 unsmoothed) and 0.20 (0.26 unsmoothed), for (a) and (b), respectively. The 10 g kg^{-1} isopleth of water vapor at 10 m above the ground at the initial model time is drawn for reference.

dryline. It was anticipated that an increase in humidity east of the dryline would lead to an increase in precipitation by way of advection into convective regions. It is less clear why humidity west of the dryline is as important. Possible explanations include an enhancement of convergence along the dryline due to a buoyancy effect, or a mixing of air into the vertical on the west side of the dryline followed by an advection of this air over the top of the dryline into the region that had convection.

In Fig. 7 sensitivity fields are plotted using the same response function definition used for Fig. 6, but with respect to soil moisture perturbations. For both positive and negative 0.01 $m^3\ m^{-3}$ volumetric soil moisture perturbations, Fig. 7 shows a large area of negative sensitivity with a smaller area of positive sensitivity just north of the positive maximum. Again, the results from positive and negative perturbations are similar. For soil moisture perturbations, the sensitivity magnitude is smaller than that from boundary layer humidity perturbations (a magnitude of about 0.7 versus 1.3). The largest effect from positive soil moisture perturbations is to cause a decrease in total precipitation, which contrasts with the predominant increase in precipitation found from positive humidity perturbations. This is an interesting effect and will be explored more in section 3c.

In Fig. 8 sensitivity fields are plotted for the same response function as in the above two cases, but with respect to perturbations in meridional wind, v. The sensitivity to v is less than that due to ABL humidity or soil moisture, with a maximum nondimensional sensitivity of 0.26. The positive–negative couplet in sensitivity seen in Fig. 8, with a positive sensitivity west of the dryline and a negative sensitivity east of the dryline, implies that anticyclonic vorticity in the ABL along the dryline led to an increase in precipitation. This is another effect for which the physical explanation is not immediately clear, though it seems reasonable that it is related to dryline dynamics. Whatever the reason, convergence at the dryline would probably be more affected by perturbations in zonal wind (which we did not attempt), rather than meridional wind, as the convergence along the dryline was mostly due to the zonal gradient of the zonal wind.

c. *Effect of soil and ABL moisture on the dryline*

Figure 7 showed a negative dependence on precipitation near the dryline to soil moisture. The physical reason for this is not obvious. One plausible explanation is that perturbing the soil moisture in some locations reduces the horizontal gradient in soil moisture, which is known to be important in the formation of the dryline (Ziegler et al. 1995; Grasso 2000). Gallus and Segal (2000) notably found that drier soil enhanced outflows from storms, which led to more precipitation. It could also be that an increase in soil moisture leads to reduced surface heating, with the reduced surface heating in turn reducing the amplitude of convection.

To examine this issue in more detail, the sensitivity of two response functions that measure dryline strength to boundary layer water vapor and soil moisture are examined. The first response function is the average 10-m horizontal wind convergence in a defined region, and the second is the maximum east–west gradient of 10-m q_v in the same region. The defined region is selected to be along the dryline at the 6-h forecast time at a location not directly affected by precipitation. Figure 9 shows the sensitivity fields for dryline convergence and Fig. 10 shows those for dryline moisture gradient. Both response functions show areas of positive and negative sensitivity to both q_v and q_s perturbations.

The physical connections are evidently complex; however, in general, positive perturbations in soil moisture near and west of the dryline tend to weaken the dryline (negative sensitivities in Figs. 9a and 10a), while positive perturbations in ABL moisture near and west of the dryline tended to strengthen it (positive sensitivities in Figs. 9b and 10b). That these two forms of moisture perturbation should have an opposite effect is interesting and indicates the complexity of dryline dynamics. The hypothesis that positive soil moisture perturbations decrease dryline precipitation because of a negative effect on dryline strength is supported by the observed negative sensitivity of dryline strength to soil moisture. A possible physical mechanism is that the increased soil moisture on the west side of the dryline reduces the surface heat flux and (hence) boundary layer vertical mixing, which has the important role of transporting upper-level westerly momentum to the low levels (Schaefer 1974) thereby enhancing dryline convergence. The reduced land-breeze effect (Sun and Ogura 1979), in which the low-level temperature gradient leads to ascending motion on the warm side and a consequent circulation loop, could be another reason since a reduction in surface heat flux on the dry side of the dryline from an increase in soil moisture would be expected to reduce the temperature gradient and, thus, any circulation loops that such gradients might generate.

d. *Sensitivity of convection near the cold front*

To examine the sensitivity of precipitation along the cold front in southern Kansas and northwestern and northern Oklahoma, a response function is defined in a region encompassing this area. This response function is defined to be the total mass of rain that fell in this box (which is drawn in Figs. 11 and 12), which covers the area north and south of the Kansas–Oklahoma border.

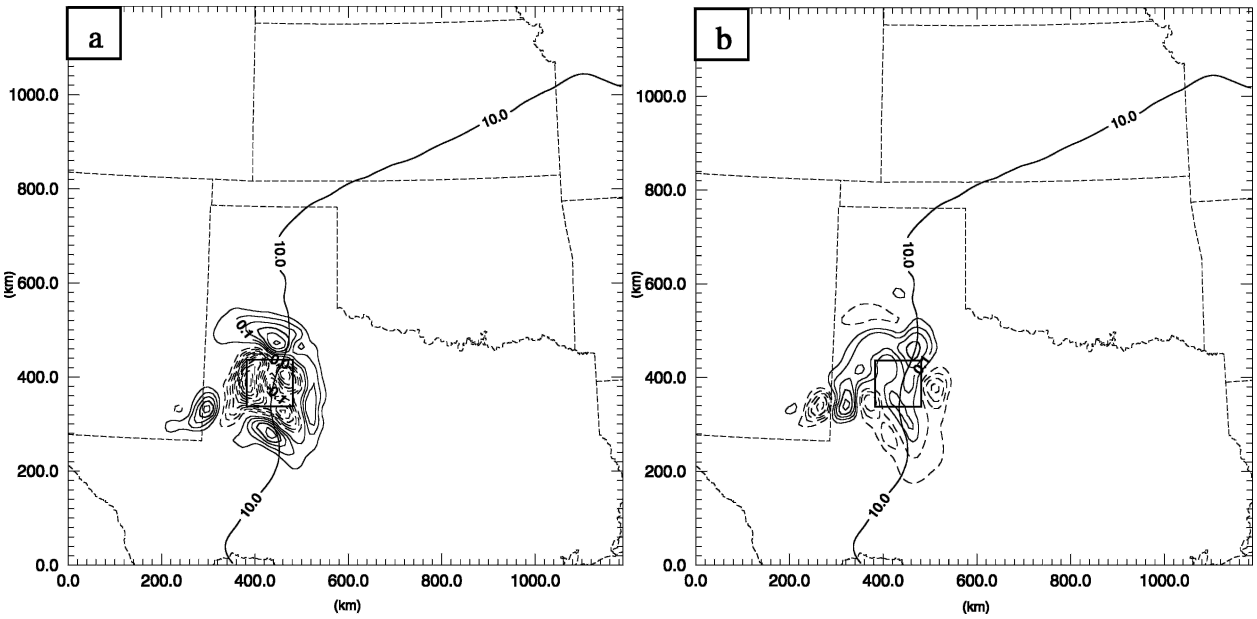

FIG. 9. Sensitivity fields for the dependence of average convergence in the indicated box to (a) initial 0.01 m^3 m^{-3} soil moisture perturbations and (b) initial 1 g kg^{-1} ABL moisture perturbations. Contour increment is 0.025. Negative contours are dashed. The 10 g kg^{-1} isopleth of water vapor at 10 m above the ground at the initial model time is drawn for reference.

The calculated nondimensional sensitivities of this response function to ABL moisture, soil moisture, and meridional ABL wind are presented in Figs. 11 and 12. In Figs. 11a and 11b the sensitivities of precipitation near the cold front to +1 and −1 g kg^{-1} ABL moisture perturbations, respectively, are shown. In this case, the sensitivity fields are quite different for positive and negative perturbations. Figure 11a shows two very strong sensitivity maxima with values exceeding 1. This is a very strong effect as it means a 1% change in ABL moisture in certain small areas led to a 1% change in the total precipitation along the cold front, which is

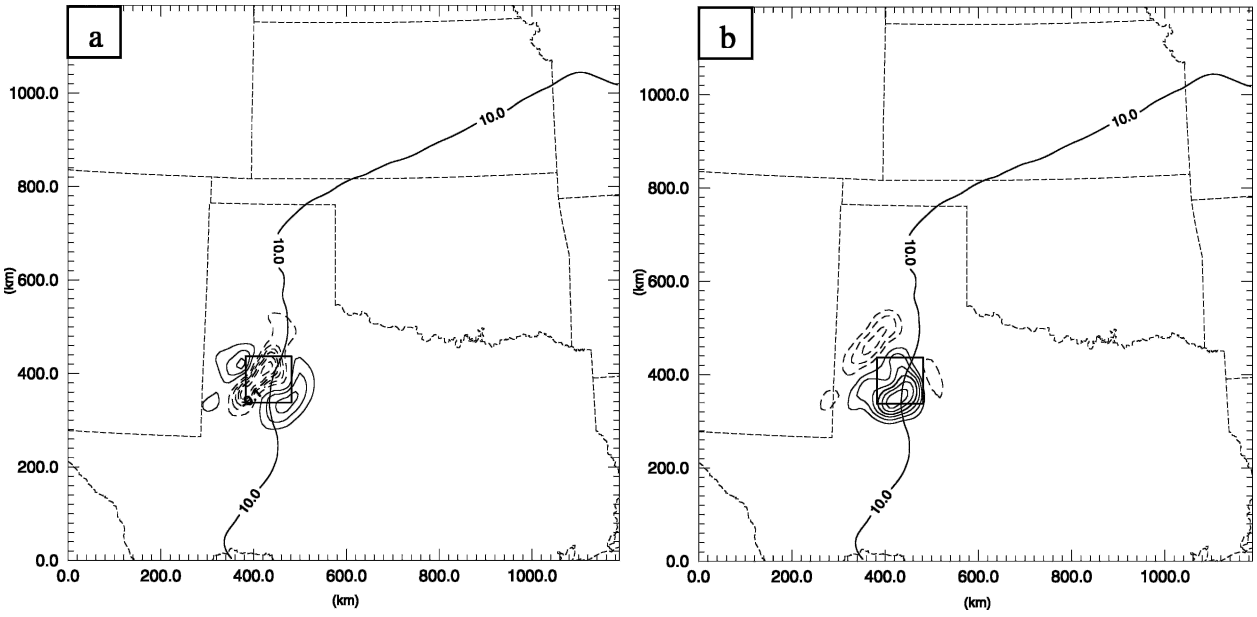

FIG. 10. Sensitivity fields for the dependence of the maximum east–west gradient of 10-m q_v in the indicated box to (a) initial 0.01 m^3 m^{-3} soil moisture perturbations and (b) initial 1 g kg^{-1} ABL perturbations. Contour increment is 0.025. Negative contours are dashed. The 10 g kg^{-1} isopleth of water vapor at 10 m above the ground at the initial model time is drawn for reference.

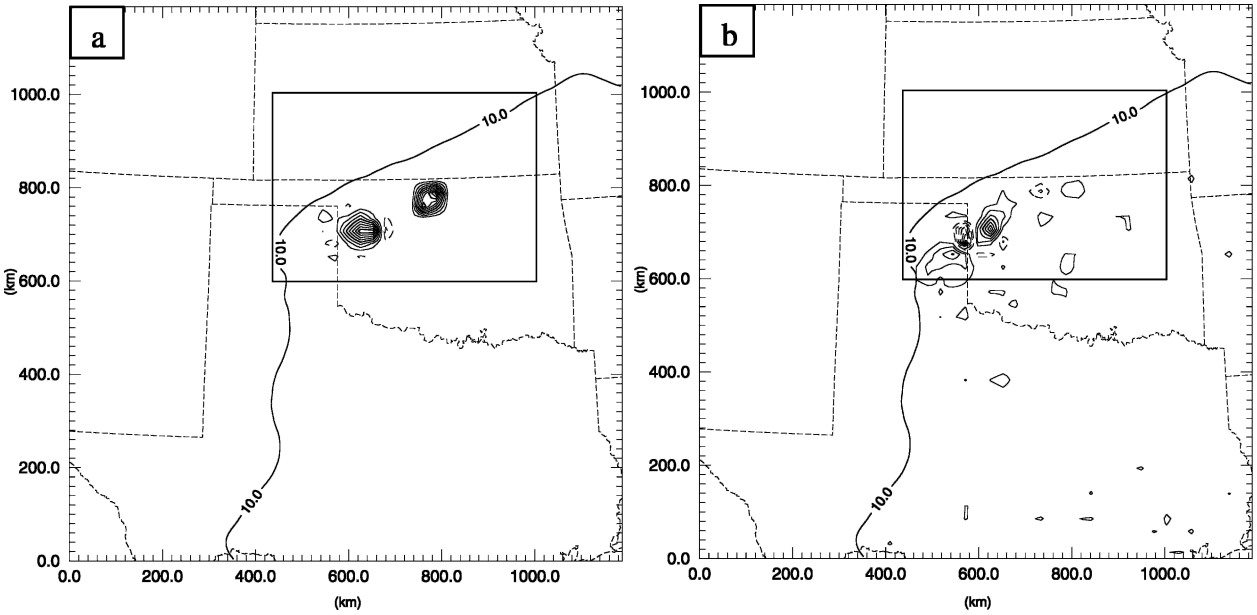

FIG. 11. Sensitivity fields for the dependence total rainfall in the indicated box to (a) initial +1 g kg^{-1} ABL moisture perturbations and (b) initial −1 g kg^{-1} ABL perturbations. Contour increment is 0.1 for (a) and 0.05 for (b). Negative contours are dashed. The maximum and minimum values for (a) are 1.03 and −0.24. The maximum and minimum values for (b) are 0.25 and −0.24. The 10 g kg^{-1} isopleth of water vapor at 10 m above the ground at the initial model time is drawn for reference.

substantial. The sensitivity of the response function calculated from negative perturbations seen in Fig. 11b is much weaker and has a different pattern than that from positive perturbations seen in Fig. 11a. This implies a significant nonlinearity in the response, or sensitivity, which will be examined further in section 3e.

In Fig. 12a is shown the sensitivity of the response function to initial +0.01 m^3 m^{-3} soil moisture pertur-

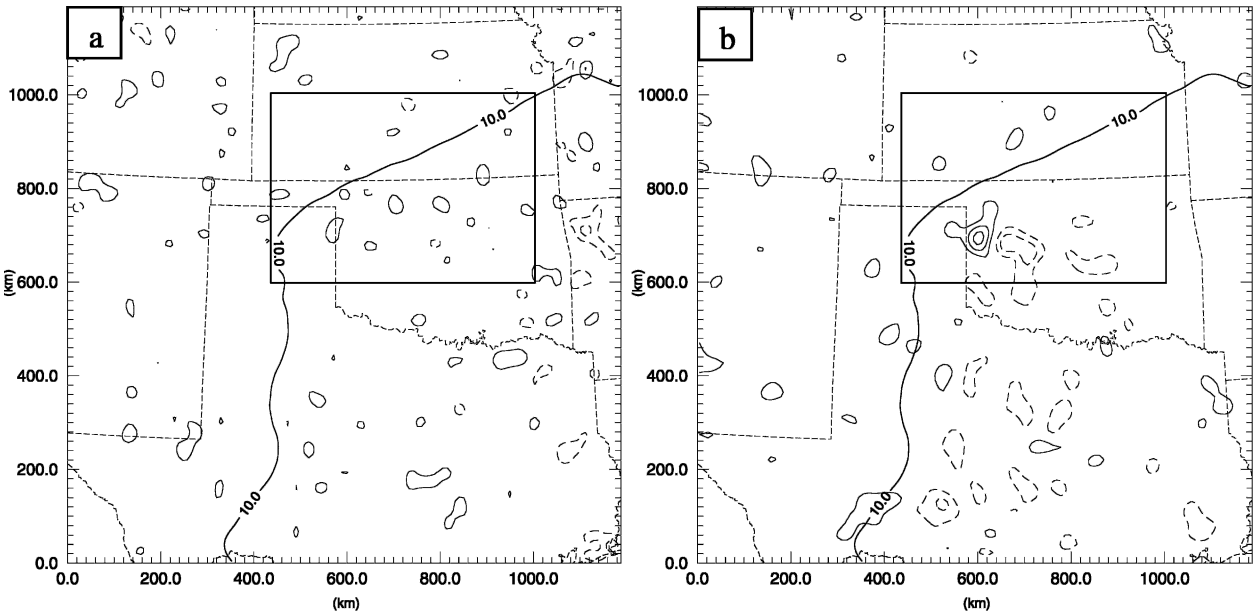

FIG. 12. Sensitivity fields for the dependence total rainfall in the indicated box to (a) initial +0.01 m^3 m^{-3} soil moisture perturbations and (b) initial +1 m s^{-1} ABL meridional wind speed perturbations. Contour increment is 0.05 for (a) and 0.01 for (b); (a) was smoothed once and (b) was smoothed three times using a nine-point smoother. Negative contours are dashed. The maximum and minimum values for (a) are 0.10 and −0.13 (0.18 and −0.13 unsmoothed). The maximum and minimum values for (b) are 0.034 and −0.028 (0.055 and −0.044 unsmoothed). The 10 g kg^{-1} isopleth of water vapor at 10 m above the ground at the initial model time is drawn for reference.

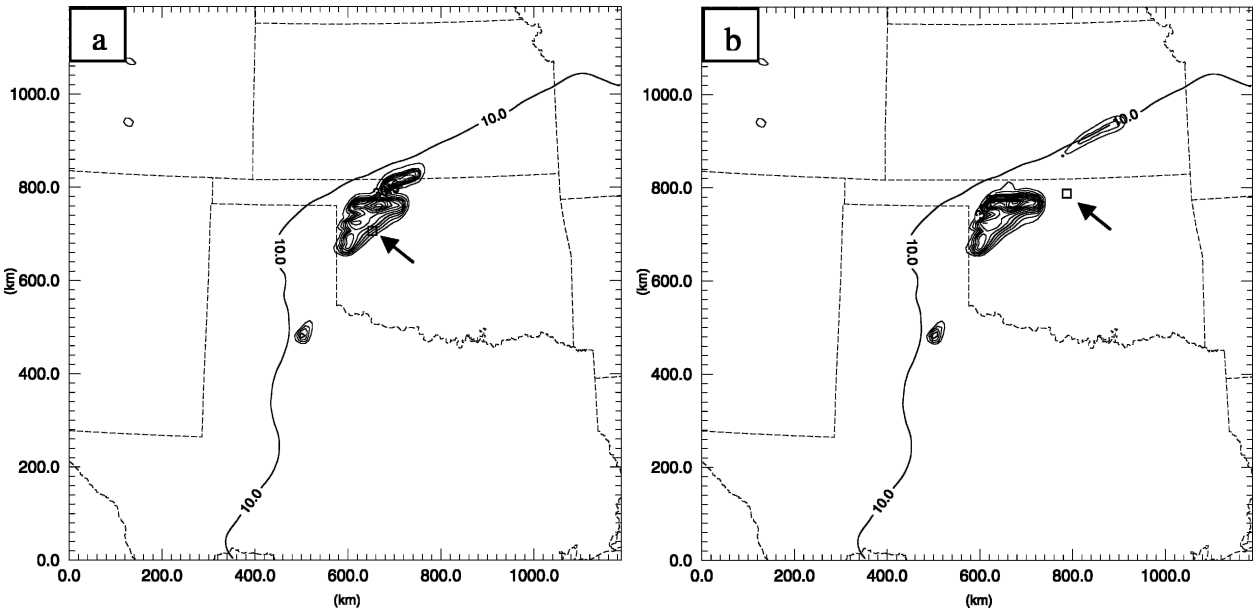

FIG. 13. Forecast accumulated precipitation that fell in two model runs with a 1 g kg^{-1} perturbation in ABL moisture at the location and of the size indicated by the drawn box in (a) northwestern Oklahoma and (b) north-central Oklahoma. The arrow in each figure indicates the location of the box. Contour increments are 15 mm. The local maximum along the Kansas–Oklahoma border in (a) is 120 mm. The local maximum in southeast Kansas in (b) is 30 mm. The 10 g kg^{-1} isopleth of water vapor at 10 m above the ground at the initial model time is drawn for reference.

bations and Fig. 12b shows the sensitivity to initial +1 m s^{-1} ABL meridional wind perturbations. The sensitivity fields from −0.01 m^3 m^{-3} soil moisture perturbations and −1 m s^{-1} v perturbations were similar to the fields from corresponding positive perturbations and are, therefore, not shown. Figure 12a exhibits mostly noise, indicating that, in sharp contrast to ABL moisture, soil moisture perturbations did not have a measurable impact on total rainfall. Figure 12b shows some sensitivity to meridional wind in the same area that ABL moisture was important (northwest Oklahoma), though the sensitivity is weaker (only 0.055 in magnitude compared with 1.0 from ABL moisture perturbations). These results are consistent with our understanding that cold fronts are more dynamically forced and are less sensitive to surface forcing than dryline systems.

e. Nonlinear sensitivities

Figure 11a showed two areas of exceptionally enhanced sensitivity of cold-frontal precipitation to positive ABL moisture perturbations. To explore this further, the actual rainfall forecasts from two of the perturbed runs with perturbations at the two maxima seen in Fig. 11a are shown in Figs. 13a and 13b. The location and size of the perturbations are shown by a box drawn in each figure. These figures can be compared with the unperturbed forecast shown in Fig. 3b. Figure 13a shows a substantial area of precipitation of over 100 mm along the Kansas–Oklahoma border, which was almost completely absent in the unperturbed run, and Fig. 13b shows an area of over 30 mm of precipitation in southeast Kansas that was completely absent in the unperturbed run. In both cases, certain convective cells only exist if the ABL moisture is perturbed in certain small areas. Small positive perturbations at some locations have led to new storms while negative perturbations had no perceptible effect. This finding should be compared with the results of Crook (1996). Crook also found that perturbations of only 1 g kg^{-1} of moisture could make the difference between getting an intense storm and getting no storm at all. Crook, however, was perturbing a sounding that represented the entire model domain. The results shown here indicate that small perturbations that are highly localized in space can have the same, highly nonlinear effect. The implication of this finding is that local differences in the analysis of ABL moisture that are within expected errors of such analyses can make substantial differences in the forecast. Irrigation of a single farm might be enough to trigger a strong convective storm, and such variations are practically not measurable by routine observational networks. This nonlinearity also suggests that, in some situations, an adjoint measure of sensitivity (which is a linear measure) would miss important effects.

4. Summary and discussion

This paper has described and applied a technique that uses a very large ensemble of forward model runs to examine the sensitivity of convection of the 24 May 2002 IHOP case to ABL water vapor and wind perturbations, and to soil moisture perturbations. This technique has proven to be very effective at revealing both significant and subtle physical sensitivities.

The large ensemble technique is fairly easy to implement, though it does require considerable computational resources. In addition to ease of implementation, it has two other significant advantages over the use of an adjoint: nonlinear sensitivity effects can be calculated, and redefining the cost function and obtaining the sensitivity fields with respect to it takes little additional effort. A principal disadvantage is that, because of computational expense, detailed three-dimensional sensitivity fields would take too many forward model runs to construct, and so we are limited to obtaining two-dimensional sensitivity fields.

In many cases, the sensitivities calculated from a VLE and an adjoint should be similar enough that the VLE technique can be used for adjoint validation. For the purpose of validation, the VLE perturbations should be made as small as possible to preserve linearity in the model's response. Thus, double precision calculations should probably be used for adjoint validation. On the other hand, for perturbations the size of initial condition analysis errors, the comparison would identify cases where the adjoint method fails, which in itself is a valuable exercise. An adjoint based on the latest version of ARPS has been developed recently with the help of automatic differentiation (Xiao et al. 2004), though full physics are not yet available with it. It is our plan to carry out intercomparison studies of sensitivities calculated with the adjoint and with forward model runs.

Results from examining sensitivities due to advection and diffusion were consistent with linear expectations and revealed the symmetry of these processes to small perturbations, implying quasi-linear behavior. To our knowledge, this symmetry has not been explicitly shown before.

The sensitivities of convection along the dryline show marked differences from those for convection along the cold front. Along the dryline, precipitation depends positively on positive ABL moisture perturbations and negatively on positive soil moisture perturbations. The reason for this difference is believed to be related to details of dryline dynamics as it is also shown that soil moisture and ABL moisture have opposite effects on dryline strength. Plausible causes for such behaviors are offered, based on current knowledge of dryline dynamics. Along the cold front, precipitation depended quite strongly on ABL moisture and had no detectable dependence on soil moisture. It was also found that the effects of soil moisture and ABL moisture are about the same on either side of the initial 1800 UTC dryline location. The fact that moisture on either side of the dryline at the time of local noon is equally important is a surprising result that we have not fully explained, though some possible reasons are offered.

TABLE 2. Summary of nondimensional sensitivities of total accumulated precipitation near the dryline and cold front to ABL moisture, soil moisture, and meridional wind component. Values are the maximum absolute value of sensitivities found from positive and negative perturbations. Soil moisture sensitivities on cold-frontal precipitation were below an approximate 0.10 noise threshold.

	ABL moisture	Soil moisture	Meridional wind
Dryline precipitation	1.5	0.85	0.26
Cold-frontal precipitation	1.03	<0.10	0.06

Table 2 summarizes the nondimensional sensitivities of precipitation along the cold front and dryline to the perturbed variables. In this table, the maximum absolute sensitivities found from either positive or negative perturbations are listed. Perturbations from ABL moisture had relatively stronger effects than those from soil moisture or ABL meridional wind component for both the dryline and cold front. However, since the ABL moisture perturbations were 1 km deep and soil moisture perturbations would only affect surface fluxes, sensitivity values are not exactly comparable, even nondimensionalized ones. Nonetheless, the strong nonlinearity seen along the cold front where entire storms were initiated from relatively small ABL moisture perturbations was not seen at all from soil moisture perturbations, which suggests the greater importance of ABL moisture, at least near the cold front for the forecast period examined here. The much longer 36-h simulations (with 12-h cycling of observations) of the same case in Holt et al. (2006) show a significant impact of soil moisture on the precipitation. As the forecast length increases, the effect of surface heat and moisture fluxes increases, effectively changing the ABL water vapor content. The fact that the effect of soil moisture perturbations had much smaller impact on cold-frontal precipitation than on dryline precipitation is consistent with our understanding that frontal systems are much more dynamically forced, while drylines are, to a large extent, driven by surface forcing.

To answer the question of how important the characterization of the water vapor field is to the forecast,

we note that for the precipitation forecast along the cold front, water vapor was clearly a critical variable. The triggering of new storms by relatively modest ABL water vapor perturbations is an effect too large for a linear estimate to be meaningful. ABL moisture would evidently need to be known to at least 1 g kg^{-1} precision to capture such effects in a forecast. It may not be practical for the field of water vapor to ever be known precisely enough to permit the accurate forecast of storm-scale details in a forecast model. For the precipitation forecast along the dryline, a nonlinear triggering effect was not seen, although it might have been, had more precipitation occurred along the dryline in the model. Nonetheless, this linear impact of water vapor is still substantial. From Fig. 6, ABL water vapor perturbations on the order of 1% over an area of 20 000 km^2 (the area of positive sensitivity seen in Fig. 6) affected the precipitation amount by about 1% that occurred over an area of about 2400 km^2 (the area of the dryline precipitation seen in Fig. 3). As the perturbations in this case were 729 km^2 in size, the effects of larger-scale perturbations (or errors in analysis) can be estimated by integrating the sensitivity field over the desired area and dividing by the size of the perturbations used. In this case, had the entire area of positive sensitivity to the southwest of the forecast precipitation seen in Fig. 6 been perturbed by 1%, the forecast precipitation would be altered by about 15%, assuming linearity would still hold with the larger-scale perturbation.

Acknowledgments. This work benefited from discussions with Jidong Gao and Ying Xiao. This research was supported primarily by NSF Grant ATM0129892. The second author was also supported by NSF Grants ATM-9909007, ATM-0331594, and EEC-0313747, a DOT–FAA grant via DOC–NOAA NA17RJ1227, and Grant 40028504 from Chinese Natural Science Foundation. The computations were performed on the National Science Foundation Terascale Computing System at the Pittsburgh Supercomputing Center.

REFERENCES

Crook, N. A., 1996: Sensitivity of moist convection forced by boundary layer process to low-level thermodynamic fields. *Mon. Wea. Rev.,* **124,** 1767–1785.

Errico, R. M., 1997: What is an adjoint model? *Bull. Amer. Meteor. Soc.,* **78,** 2577–2591.

——, 2003: The workshop on applications of adjoint models in dynamic meteorology. *Bull. Amer. Meteor. Soc.,* **84,** 795–798.

——, and T. Vukicevic, 1992: Sensitivity analysis using an adjoint of the PSU–NCAR mesoscale model. *Mon. Wea. Rev.,* **120,** 1644–1660.

Fovell, R. G., 2004: Adjoint of a parameterized moisture convection model. *Meteor. Atmos. Phys.,* **86,** 173–194.

Gallus, W. A., Jr., and M. Segal, 2000: Sensitivity of forecast rainfall in a Texas convective system to soil moisture and convective parameterization. *Wea. Forecasting,* **15,** 509–525.

Grasso, L. D., 2000: A numerical simulation of dryline sensitivity to soil moisture. *Mon. Wea. Rev.,* **128,** 2816–2834.

Hall, M. C. G., and D. G. Cacuci, 1982: Sensitivity analysis of a radiative–convective model by the adjoint method. *J. Atmos. Sci.,* **39,** 2038–2050.

——, and ——, 1983: Physical interpretation of the adjoint functions for sensitivity analysis of atmospheric models. *J. Atmos. Sci.,* **40,** 2537–2546.

Holt, T. R., D. Niyogi, F. Chen, K. Manning, M. A. LeMone, and A. Qureshi, 2006: Effect of land–atmosphere interactions on the IHOP 24–25 May 2002 convection case. *Mon. Wea. Rev.,* **134,** 113–133.

Kim, H. M., M. C. Morgan, and R. E. Morss, 2004: Evolution of analysis error and adjoint-based sensitivities: Implications for adaptive observations. *J. Atmos. Sci.,* **61,** 795–812.

Kleist, D. T., and M. C. Morgan, 2005: Intrepretation of the structure and evolution of adjoint-derived forecast sensitivity gradients. *Mon. Wea. Rev.,* **133,** 466–484.

Mullen, S. L., and D. P. Baumhefner, 1994: Monte Carlo simulations of explosive cyclogenesis. *Mon. Wea. Rev.,* **122,** 1548–1567.

Park, S. K., and K. K. Droegemeier, 1999: Sensitivity analysis of a moist 1D Eulerian cloud model using automatic differentiation. *Mon. Wea. Rev.,* **127,** 2180–2196.

Schaefer, J. T., 1974: A simulative model of dryline motion. *J. Atmos. Sci.,* **31,** 956–964.

Sun, W.-Y., and Y. Ogura, 1979: Boundary-layer forcing as a possible trigger to a squall line formation. *J. Atmos. Sci.,* **36,** 235–254.

Wakimoto, R. M., H. V. Murphey, E. V. Browell, and S. Ismail, 2006: The "triple point" on 24 May 2002 during IHOP. Part I: Airborne Doppler and LASE analyses of the frontal boundaries and convection initiation. *Mon. Wea. Rev.,* **134,** 231–250.

Weckwerth, T. M., and Coauthors, 2004: An overview of the International H_2O Project (IHOP_2002) and some preliminary highlights. *Bull. Amer. Meteor. Soc.,* **85,** 253–277.

Xiao, Y., M. Xue, W. J. Martin, and J. D. Gao, 2004: Development of an adjoint for a complex atmospheric model, the ARPS, using TAF. *Automatic Differentiation: Applications, Theory, and Implementations,* H. M. Bücker et al., Eds., Springer, 263–272.

Xue, M., and W. J. Martin, 2006: A high-resolution modeling study of the 24 May 2002 dryline case during IHOP. Part II: Horizontal convective rolls and convective initiation. *Mon. Wea. Rev.*, **134,** 172–191.

——, K. K. Droegemeier, and V. Wong, 2000: The Advanced Regional Prediction System (ARPS)—A multiscale nonhydrostatic atmospheric simulation and prediction tool. Part I: Model dynamics and verification. *Meteor. Atmos. Phys.,* **75,** 161–193.

——, and Coauthors, 2001: The Advanced Regional Prediction System (ARPS)—A multiscale nonhydrostatic atmospheric simulation and prediction tool. Part II: Model physics and applications. *Meteor. Atmos. Phys.,* **76,** 143–165.

——, D. Wang, J. Gao, K. Brewster, and K. Droegemeir, 2003: The Advanced Regional Prediction System (ARPS), storm-scale numerical weather prediction and data assimilation. *Meteor. Atmos. Phys.,* **82,** 139–170.

Zalesak, S. T., 1979: Fully multidimensional flux-corrected transport algorithms for fluids. *J. Comput. Phys.,* **31,** 335–362.

Ziegler, C. L., W. J. Martin, R. A. Pielke, and R. L. Walko, 1995: A modeling study of the dryline. *J. Atmos. Sci.,* **52,** 263–285.